Journal of the Taiwan Institute of Chemical Engineers 73 (2017) 86–92

Contents lists available at ScienceDirect

Journal of the Taiwan Institute of Chemical Engineers

journal homepage: www.elsevier.com/locate/jtice

Development of mathematical programs for evaluating dynamic and temporal flexibility indices based on KKT conditions

Ruei-Shing Wu, Chuei-Tin Chang*

Department of Chemical Engineering, National Cheng Kung University, Tainan 70101, Taiwan

ARTICLE INFO

Article history:
Received 15 April 2016
Revised 3 September 2016
Accepted 7 September 2016
Available online 16 September 2016

Keywords:
Flexibility index
Karush–Kuhn–Tucker conditions
Dynamic programing model

ABSTRACT

In addition to the economic criteria, it is equally important to consider operational flexibility in a realistic process design. Two quantitative measures, *i.e.*, the dynamic and temporal flexibility indices, have already been proposed in the past to characterize the batch or unsteady operations, and the corresponding multi-level dynamic programming models have also been developed for calculating such metrics. However, the available algorithms are still not mature enough to ensure computation accuracy and/or to guarantee convergence in every optimization run. These drawbacks have been circumvented in the present study by converting the above models into single-level ones on the basis of the Karush–Kuhn–Tucker (KKT) conditions. The numerical results obtained in several case studies are reported in this paper to demonstrate the benefits of the proposed solution strategy.

1. Introduction

Dealing with uncertainties is one of the practical issues in designing chemical plants. The so-called uncertainties may arise from exogenous disturbances (such as those in feed qualities, product demands and environmental conditions, etc.) or internal model parameters (such as heat transfer coefficient, reaction rate constants and other physical properties, etc.) [1–4]. The ability of a process to maintain feasible operation despite uncertain deviations from the nominal states is often referred to as its operational flexibility and a steady-state flexibility index was first defined mathematically by Swaney and Grossmann [5,6] for use as a gauge of the feasible region in the parameter space. However, this original metric is adopted primarily for assessing the operational feasibility of any given continuous process. Dimitriadis and Pistikopoulos [7] suggested that a batch or unsteady operation must be analysed differently and proposed to use a so-called *dynamic flexibility index* according to the differential algebraic equations (DAEs). This practice is more rigorous than that based on the steady-state model for the obvious reason that the flexibility of a process cannot properly be described without considering its transient behavior under the influence of external disturbances. In an earlier study, Brengel and Seider [8] advocated the need for design and control integration. Dimitriadis et al. [9] studied the operational feasibility issue for safety verification purpose, while Zhou et al. [10] utilized a similar approach to assess the operational flexibility of batch system.

In order to calculate the aforementioned dynamic flexibility index, the nominal values of uncertain parameters and the anticipated positive and negative deviations in these parameters are assumed to be available at every instance over the time horizon. The corresponding index can then be computed on the basis of dynamic system model and such a priori information. On the other hand, while an ill designed system may become inoperable due to instantaneous disturbances, the cumulative effects of temporary parameter variations can also lead to serious consequences. To address this practical issue, a mathematical programming model was proposed by Adi and Chang [11] to evaluate the corresponding *temporal flexibility index*. They applied this performance measure in the designs of the solar-driven membrane distillation desalination system [12] and the hybrid power generation systems [13].

From the above discussions, it can be noted that the dynamic and temporal flexibility indices may complement one another to characterize a given unsteady process and, thus, both could be considered in design. However, although the implementation procedure of these performance measures has already been adequately developed, their numerical values cannot be reliably calculated with the existing heuristic optimization algorithms [14]. In present study, the theoretical foundation has been laid on a more solid ground by transforming the traditional multi-level optimization problem into a single-level one. Specifically, the Karush–Kuhn–Tucker (KKT) conditions of the lower-level optimization problem were first derived rigorously and the trapezoidal integration formula then applied to discretize the corresponding equality and inequality constraints. As a result, the transformed optimization problem can be solved more easily and accurately with available commercial software.

* Corresponding author.
E-mail address: ctchang@mail.ncku.edu.tw (C.-T. Chang).

http://dx.doi.org/10.1016/j.jtice.2016.09.009
1876-1070/

The remaining of this paper is organized as follows. The conventional formulation is first reviewed in Section 2. The different mathematical programming models for evaluating the dynamic and temporal flexibility indices are formulated accordingly in Section 3, and the derivation of KKT conditions is then outlined in Section 4. The trapezoidal rule used for discretizing the resulting model is illustrated in Section 5. Two examples are provided in Section 6 to demonstrate the feasibility and effectiveness of the proposed method. Finally, in Section 7, conclusions are drawn from these case studies.

2. Process model

All equality constraints in a dynamic model can be expressed in a general form as

$$h_i\left(\mathbf{d}, \mathbf{z}(t), \mathbf{x}(t), \dot{\mathbf{x}}(t), \boldsymbol{\theta}(t)\right) = \dot{x}_i(t) - \varphi_i\left(\mathbf{d}, \mathbf{z}(t), \mathbf{x}(t), \boldsymbol{\theta}(t)\right) = 0, \quad \mathbf{x}(0) = \mathbf{x}^0 \tag{1}$$

where, i is the numerical label of an equality constraint; $\mathbf{d}$ represents a constant vector in which all design specifications are stored; $\mathbf{z}$ denotes the vector of all adjustable control variables; $\mathbf{x}$ is the vector of all state variables; $\boldsymbol{\theta}$ denotes the vector of all uncertain parameters. Notice that h_i is expressed with various functions of time and it is usually established to model the dynamic behavior of an unsteady process over a given horizon (say,$0 < t \le H$). Similarly, the inequality constraints can be written as

$$g_j\left(\mathbf{d}, \mathbf{z}(t), \mathbf{x}(t), \boldsymbol{\theta}(t)\right) \le 0 \tag{2}$$

where, j is the numerical label of an inequality constraint and g_j is also a functional defined over the aforementioned horizon. Note that Eq. (2) is often adopted to reflect the actual physical and/or chemical limits.

The anticipated upper and lower bounds of the uncertain parameters should be incorporated in the present model as

$$\boldsymbol{\theta}^N(t) - \Delta\boldsymbol{\theta}^-(t) \le \boldsymbol{\theta}(t) \le \boldsymbol{\theta}^N(t) + \Delta\boldsymbol{\theta}^+(t) \tag{3}$$

These bounds may be extracted directly from historical operation records in the chemical plant under consideration. To facilitate clear explanation, let us instead consider the weather information as an example. Specifically, by setting H to be 24 h and t to be the hour of a day, $\boldsymbol{\theta}^N(t)$, $\Delta\boldsymbol{\theta}^-(t)$ and $\Delta\boldsymbol{\theta}^+(t)$ may be established according to the largest range of *hourly* rainfall data collected every day over months.

If the cumulated quantities of the above parameters over time are recorded, the following extra inequalities may also be adopted to better characterize the uncertainties

$$-\Delta\boldsymbol{\Theta}^- \le \int_0^H \left[\boldsymbol{\theta}(\tau) - \boldsymbol{\theta}^N(\tau)\right]d\tau \le +\Delta\boldsymbol{\Theta}^+ \tag{4}$$

Again for illustration purpose, let us consider the climate statistics. The values of $\Delta\boldsymbol{\Theta}^+$ and $\Delta\boldsymbol{\Theta}^-$ in this case can now be estimated according to the *daily* rainfall data which are usually also available. Since the uncertain parameters usually do not always stay at the upper (or lower) limits throughout the entire horizon, one would expect $\Delta\boldsymbol{\Theta}^- \le \int_0^H \Delta\boldsymbol{\theta}^-(\tau)d\tau$ and $\Delta\boldsymbol{\Theta}^+ \le \int_0^H \Delta\boldsymbol{\theta}^+(\tau)d\tau$.

3. Dynamic and temporal flexibility indices

Let us consider a feasibility functional, whose scalar value can be determined as follows:

$$\psi\left(\mathbf{d}, \boldsymbol{\theta}(t)\right) = \min_{\mathbf{x}(t),\mathbf{z}(t)} \max_{j,t} g_j\left(\mathbf{d}, \mathbf{z}(t), \mathbf{x}(t), \boldsymbol{\theta}(t)\right) \tag{5}$$

subject to the equality constraints given in Eq. (1). Note that the given system should be always operable if $\Psi \le 0$.

In order to evaluate the dynamic flexibility index, let us introduce a scalar variable δ to adjust the ranges of the transient variations in Eq. (3), *i.e.*

$$\boldsymbol{\theta}^N(t) - \delta\Delta\boldsymbol{\theta}^-(t) \le \boldsymbol{\theta}(t) \le \boldsymbol{\theta}^N(t) + \delta\Delta\boldsymbol{\theta}^+(t) \tag{6}$$

The corresponding performance measure, *i.e.*, the dynamic flexibility index, [7] can be computed accordingly with the following model:

$$FI_d = \max \delta \tag{7}$$

subject to Eq. (6) and

$$\max_{\boldsymbol{\theta}(t)} \psi\left(\mathbf{d}, \boldsymbol{\theta}(t)\right) \le 0 \tag{8}$$

On the other hand, the aforementioned scalar variable can be incorporated into Eq. (4) instead to take in account of the accumulated effects of uncertain parameters in non-steady operations, *i.e.*

$$-\delta\Delta\boldsymbol{\Theta}^- \le \int_0^H \left[\boldsymbol{\theta}(\tau) - \boldsymbol{\theta}^N(\tau)\right]d\tau \le +\delta\Delta\boldsymbol{\Theta}^+ \tag{9}$$

Consequently, the corresponding temporal flexibility index [11] can be computed as follows:

$$FI_t = \max \delta \tag{10}$$

subject to Eqs. (3), (8) and (9).

4. Karush–Kuhn–Tucker conditions

The mathematical program for computing the feasibility functional defined in Eq. (5) can be posed alternatively by introducing another scalar variable $u(t)$, *i.e.*

$$\psi\left(\mathbf{d}, \boldsymbol{\theta}(t)\right) = \min_{\mathbf{x}(t),\mathbf{z}(t),u(t)} u(t)|_{t=H} \tag{11}$$

subject to the equality constraints in Eq. (1), and also

$$\dot{u}(t) = 0 \tag{12}$$

$$g_j\left(\mathbf{d}, \mathbf{z}(t), \mathbf{x}(t), \boldsymbol{\theta}(t)\right) \le u(t) \tag{13}$$

To facilitate derivation of Karush–Kuhn–Tucker (KKT) conditions for this functional optimization problem, let us rewrite Eq. (1) in vector form as

$$\boldsymbol{\varphi}\left(\mathbf{d}, \mathbf{z}(t), \mathbf{x}(t), \boldsymbol{\theta}(t)\right) - \dot{\mathbf{x}}(t) = \mathbf{0} \tag{14}$$

An aggregated objective functional can then be constructed by introducing Lagrange multipliers to incorporate of all constraints, *i.e.*

$$L = u(H) + \int_0^H \left\{\mu_1(t)[0 - \dot{u}] + \boldsymbol{\mu}_2^T(t)\left[\boldsymbol{\varphi} - \dot{\mathbf{x}}\right] + \boldsymbol{\lambda}^T(t)[\mathbf{g} - u\mathbf{1}]\right\}dt \tag{15}$$

where, the multipliers for all equality constraints are real while those for inequalities should be non-negative; $\mathbf{1}$ is a vector in which all elements are one (1). By taking the first variation of L and then set it to zero, one can produce the following four groups of necessary conditions according to Eqs (11)–(15):

(i) $\mu_1(0)=0$, $\mu_1(H)=1$, $\mathbf{x}(0)=\mathbf{x}_0$, $\boldsymbol{\mu}_2(H)=\mathbf{0}$;
(ii) $\dot{\boldsymbol{\mu}}_2 = -\boldsymbol{\mu}_2^T\left(\frac{\partial\boldsymbol{\varphi}}{\partial\mathbf{x}}\right) - \boldsymbol{\lambda}^T\left(\frac{\partial\mathbf{g}}{\partial\mathbf{x}}\right)$, $\dot{\mu}_1 = \boldsymbol{\lambda}^T\mathbf{1}$;
(iii) $\boldsymbol{\mu}_2^T\left(\frac{\partial\boldsymbol{\varphi}}{\partial\mathbf{z}}\right) + \boldsymbol{\lambda}^T\left(\frac{\partial\mathbf{g}}{\partial\mathbf{z}}\right) = \mathbf{0}^T$;
(iv) $\dot{\mathbf{x}} = \boldsymbol{\varphi}$, $\dot{u} = 0$, $\boldsymbol{\lambda}^T(\mathbf{g} - u\mathbf{1}) = 0$, $\boldsymbol{\lambda} \ge \mathbf{0}$.

Since at least one of the inequality constraints must be active at certain time instance when the extremum is reached, it is necessary to force $u(t)$ to be zero over $[0, H]$. Thus, the conditions in (iv) can be modified as follows:

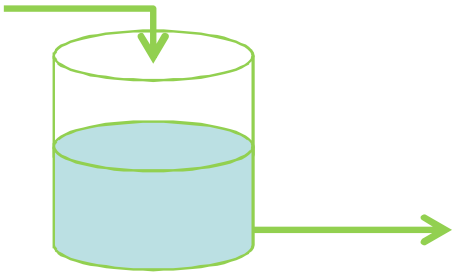

Fig. 1. A buffer vessel.

(v) $\dot{\mathbf{x}} = \boldsymbol{\varphi}, u = 0, \boldsymbol{\lambda}^T\mathbf{g} = 0, \boldsymbol{\lambda} \geq \mathbf{0}, \mathbf{g} \leq \mathbf{0}$.

Therefore, the dynamic and temporal flexibility indices can be determined respectively by minimizing δ, subject to the common conditions specified in (i)–(iii), (v), and also the aforementioned two separate sets of constraints imposed upon the uncertain parameters, *i.e.*, Eq. (6) for computing the dynamic flexibility index and Eqs. (3) and (9) for the temporal flexibility index.

5. Trapezoidal integration rule

To estimate the integrals of $\boldsymbol{\varphi}$, let us divide the horizon [0, H] into M equal intervals and label their end points sequentially as $p = 1, 2, \ldots, M$. Thus, the length of each time interval should be H/M (denoted as Δt). By applying the trapezoidal rule, one can obtain

$$\mathbf{x}(t_p) = \mathbf{x}(t_{p-1}) + \frac{\Delta t}{2}[\boldsymbol{\varphi}(\mathbf{d}, \mathbf{x}(t_{p-1}), \mathbf{z}(t_{p-1}), \boldsymbol{\theta}(t_{p-1})) + \boldsymbol{\varphi}(\mathbf{d}, \mathbf{x}(t_p), \mathbf{z}(t_p), \boldsymbol{\theta}(t_p))] \quad (16)$$

where, $\mathbf{x}(t_0) = \mathbf{x}(0) = \mathbf{x}_0$. Note that the inequality constraints in Eq. (2) can also be discretized according to the aforementioned points.

6. Case studies

Additional slack and binary variables can then be adopted to reformulate the last three conditions in (v), *i.e.*, $\boldsymbol{\lambda}^T\mathbf{g} = 0$, $\boldsymbol{\lambda} \geq \mathbf{0}$ and $\mathbf{g} \leq \mathbf{0}$, so as to construct two distinct MINLP models for evaluating the dynamic and temporal flexibility indices, respectively, on the basis of the aforementioned KKT conditions and trapezoidal integration rule. Two examples are presented in the sequel to demonstrate the feasibility and effectiveness of this approach. Solver SBB in GAMS 23.9.5 was adopted to perform the needed optimization runs on a PC equipped with Intel core i7-4770 3.4 GHz.

6.1. Example 1: periodic buffer operation

Let us consider the buffer tank in Fig. 1. The corresponding dynamic model can be written as

$$A\frac{dh}{dt} = \theta(t) - k\sqrt{h} \quad (17)$$

where, h denotes the height of liquid level (m); A (= 5 m^2) is the cross-sectional area of the tank; k (= $\sqrt{5}$/10m$^{5/2}$/min) is a proportionality constant; θ denotes the feed flow rate (m^3/min) and it is treated as the only uncertain parameter in the present example. To fix ideas, the following upper and lower limits are adopted in the flexibility analysis:

(1) The height of tank is 10 m, *i.e.*, $h \leq 10$.
(2) Due to the operational requirement of downstream unit(s), the outlet flow rate of buffer tank must be kept above $\sqrt{5}/10\ m^3$/min. Thus, the minimum allowable height of its liquid level should be 1 m, *i.e.*, $1 \leq h$.

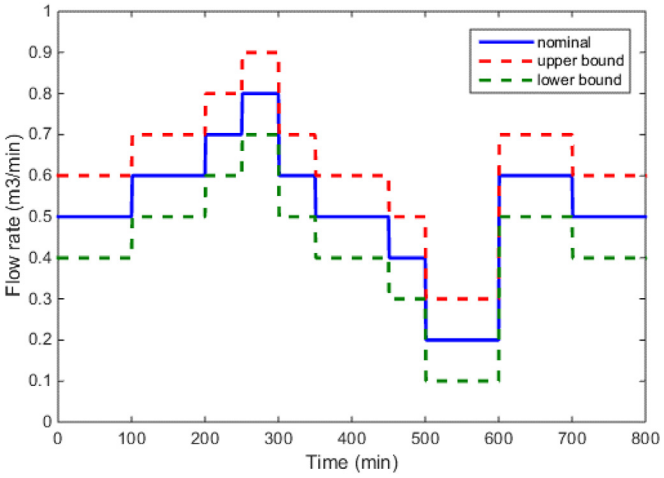

Fig. 2. Nominal feed rate and its upper and lower limits for periodic operation.

Table 1
Computation times needed to evaluate the dynamic and temporal flexibility indices by solving two alternative models in Example 1 ($A = 5$ m^2).

Programming model	FI_d (s)	FI_t (s)
KKT	28.6	5.8
Vertex	1	1920

(3) The time horizon covers a period of 800 min, *i.e.*, $0 \leq t \leq 800$.

Let us next assume that, over a period of 800 min, the nominal feed rate, the expected upper and lower bounds can be determined a priori (see Fig. 2). Note that the expected positive and negative deviations at any time are set at 0.1 (m^3/min). To facilitate computation of temporal flexibility index, let us also assign the accumulated positive and negative deviations in liquid volumes to be $\Delta\Theta^+ = \Delta\Theta^- = 20.0\ \text{m}^3$.

Based on an initial height of 5 m, the corresponding dynamic flexibility index was found to be 0.368 while the temporal flexibility index 0.185. The worst-case scenarios in both cases reached the lower bound of water level around 600 min. It was also observed that the latter index ($FI_t = 0.185$) is associated with the scenario that the feed rate increases to its upper bound between 563 and 600 min. For the purposes of raising these indices to 1, one can adjust the cross-sectional area of the buffer tank or improve the control quality of the upstream feed stream. To be more specific, the required areas for these two criteria should be enlarged to 8.25 and 6.95 m^2, respectively. It can be also noted that the former index ($FI_d = 0.368$) can be raised to 1 if the range of expected deviations were narrowed by 0.368.

Finally, the computation performance of the proposed method has been compared with that of the extended vertex method developed by Kuo and Chang. [14] It was found that, in this example, the flexibility indices obtained with both approaches were almost identical in every scenario. Table 1 summarizes the corresponding computation times needed in typical optimization runs. It can be observed that, although it took a somewhat longer time to calculate FI_d with the proposed method, the computation load for evaluating FI_t was reduced tremendously by solving a programming model that includes the KKT conditions.

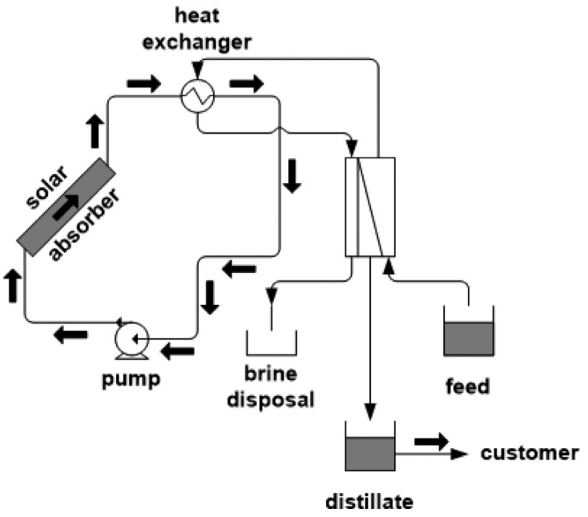

Fig. 3. SMDD process.

6.2. Example 2: solar-driven membrane distillation desalination (SMDD) process

Let us next consider the SMDD process in Fig. 3, which include the solar absorber, the counter-flow heat exchanger, the air gap membrane distillation (AGMD) modules, and the distillate tank, are connected to form two separate processing routes for seawater desalination and solar energy conversion, respectively. Clearly a realistic system design must be fully functional in the presence of uncertain sunlight radiation and unpredictable freshwater demand. To facilitate rigorous flexibility analyses, the mathematical models of all units in this system must be first obtained and a brief summary of the ones adopted in the present example is given below. Furthermore, for illustration clarity, an Appendix is provided at the end of this paper to define all symbols in these models and to specify all parameter values used in calculations.

6.2.1. Unit models

- Solar absorber

The solar energy is converted into heat using solar absorber, assuming that the fluid velocities in all absorber tubes are the same and heat loss is negligible. The corresponding transient energy balance can be written as

$$\frac{dT_{f,\mathrm{SAout}}}{dt} = -\frac{\dot{m}_{f,\mathrm{SA}}}{M_{f,\mathrm{SA}}}\left(T_{f,\mathrm{SAout}} - T_{f,\mathrm{SAin}}\right) + \frac{A_{\mathrm{SA}} I(t)}{M_{f,\mathrm{SA}} Cp^{L}} \tag{18}$$

where $T_{f,\mathrm{SAin}}$ and $T_{f,\mathrm{SAout}}$ denote the inlet and outlet temperatures (°C) of the solar absorber respectively; $M_{f,\mathrm{SA}}$ denotes the total mass of operating fluid in the solar absorber (kg); $\dot{m}_{f,\mathrm{SA}}$ denotes the overall mass flow rate of operating fluid in solar absorber (kg/hr); A_{SA} is the exposed area of solar absorber (m^2); Cp^L is the heat capacity of operating fluid (J/kg°C); $I(t)$ is the solar irradiation rate per unit area (W/m^2). The outlet temperature of the solar absorber should be less than the maximum allowable outlet temperature $T_{SA\mathrm{out,max}}$ (= 100 °C), *i.e.*, $T_{f,SA\mathrm{out}} \le T_{SA\mathrm{out,max}}$.

- Counter-flow heat exchanger

The hot fluid used in heat exchanger comes from the solar absorber, and the cold fluid is the seawater. The heat exchanger is assumed to be steady and there is no any heat loss. Hence, the formulation of heat exchanger can be written as

$$\dot{m}_{f,MD}\left(T_{f,\mathrm{HX,CLout}} - T_{f,\mathrm{HX,CLin}}\right) = \dot{m}_{f,\mathrm{HX,HL}}\left(T_{f,\mathrm{HX,HLin}} - T_{f,\mathrm{HX,HLout}}\right) \tag{19}$$

where $\dot{m}_{f,\mathrm{HX,HL}}$ is the mass flow rate of hot fluid (kg/hr); $T_{f,\mathrm{HX,HLin}}$ and $T_{f,\mathrm{HX,HLout}}$ denote the inlet and outlet temperatures of hot fluid respectively (°C); $\dot{m}_{f,\mathrm{MD}}$ is the mass flow rate of seawater in membrane distillation loop (kg/hr) treated as a control variable in this work, which expected deviation is ±10% from its nominal value; $T_{f,\mathrm{HX,CLin}}$ and $T_{f,\mathrm{HX,CLout}}$ denote the inlet and outlet temperatures of cold fluid, respectively (°C).

- Air gap membrane distillation (AGMD)

A simplified model is adopted in this study for characterizing the AGMD unit. It is assumed that the mass flux of distillate across the membrane is a function of the rate of energy input and can be expressed as

$$N_{mem} \cong \frac{\dot{m}_{f,MD} Cp_f^L \left(T_{f,HX,CLout} - T_{f,HX,CLin}\right)}{STEC \cdot A_{MD} \cdot n_{AGMD}} \tag{20}$$

where N_{mem} denotes the distillate flux (kg/m^2 hr); A_{MD} (=10 m^2) is the membrane area of a standard AGMD module; n_{AGMD} (=4) is the total number of standard modules, which value has to be calculated according to historical maximum daily water demand; STEC is the *specific thermal energy consumption constant* (kJ/kg), which can be considered as the ratio between energy supply by the heat exchanger and the mass of the distillate produced.

- Distillate tank

The distillate tank is acting as the buffer tank for the uncertain water demand. The corresponding model can be expressed as

$$\rho A_{DT} \frac{dh_{DT}}{dt} = n_{AGMD} N_{mem} A_{MD} - w_D \tag{21}$$

where ρ is the distillate density (kg/m^3); A_{DT} (= 0.35 m^2)is the cross-sectional area of distillate tank (m^2); h_{DT} is the level of liquid in the distillate tank (m); w_D is the outlet flow (kg/hr), and note that the first term on the right hand side of Eq. (21) denotes the inlet flow produced by the AGMD unit. Finally, the level of liquid in the distillate should be maintained within a specific range, *i.e.*, $h_{DT,\mathrm{lo}} \le h_{DT} \le h_{DT,\mathrm{up}}$, where $h_{DT,\mathrm{lo}}$ (=0 m) and $h_{DT,\mathrm{up}}$ (= 2.14 m) represent the given lower and upper bounds.

6.2.2. Flexibility analyses

There are two uncertain parameters considered in this case study. One is the solar irradiation rate $I(t)$, and the other is the water demand rate w_D, The corresponding nominal profile, expected upper and lower bounds are depicted respectively in Figs. 4 and 5. Note that the expected positive and negative deviations at any time are both set at 10% of the nominal value for these uncertainty parameters. Let us also assign the accumulated positive and negative deviations in solar irradiation and in water demand to be $\Delta\Theta_I{}^+ = \Delta\Theta_I{}^- = 2\times10^6$ W and $\Delta\Theta_{DTout}{}^+ = \Delta\Theta_{DTout}{}^- = 40$ kg, respectively. Finally, let us assume the time horizon covers a period of 1440 min, *i.e.*, $0 \le t \le 1440$.

It should be also noted that the solar absorber should be sized according to the AGMD capacity. To determine proper area of solar absorber, the following *utilization ratio* (φ_{util}) should be first stipulated:

$$\phi_{util} = \frac{\text{maximum supply rate of solar energy}}{\text{maximum consumption rate of thermal energy}} = \frac{A_{SA} I^{\max}}{m_{MD}^{\max} Cp^{L}\left(T_{f,\mathrm{HX,CLout}}^{\max} - T_{f,\mathrm{HX,CLin}}\right)} \tag{22}$$

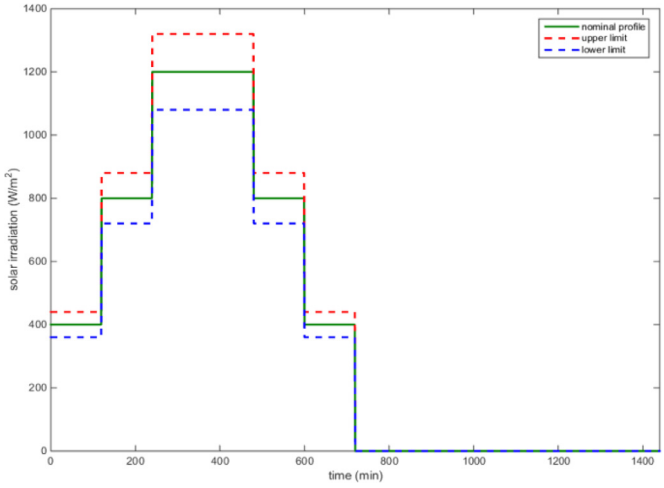

Fig. 4. Solar irradiation profile.

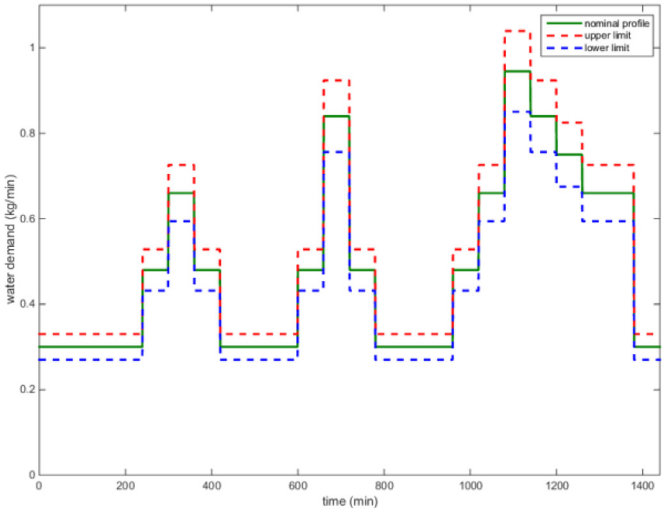

Fig. 5. Water demand profile.

Table 2
Optimization results obtained in Example 2.

Case no.	1	2	3	4
φ_{util}	0.683	0.75	1	1.04
FI_d	0 (0)	0.415(0.415)	1.077(1.077)	0.664(0.664)
$g_j=0$	$h_{DT,lo}$	$h_{DT,lo}$	$T_{SA\,out,max}$	$T_{SA\,out,max}$
FI_t	0 (0)	0.723(0.723)	–	0.242(0.242)
$g_j=0$	$h_{DT,lo}$	$h_{DT,lo}$	–	$T_{SA\,out,max}$

In this example, the denominator of this ratio is always set to be 1,559,250 kJ/hr. Based on an initial liquid height of 0.4285 m in distillate tank, the dynamic flexibility indices and temporal flexibility indices can be computed for different utilization ratios. Table 2 summarizes the optimization results computed based on the method presented in this work and the corresponding results obtained by the conventional vertex method can also be found in the corresponding parentheses.

For Case 1 ($\varphi_{util}=0.683$, $FI_d=0.0$), no deviations from nominal value are tolerable. This result is due to the fact that the solar energy absorbed is just enough to meet the nominal water demand. Obviously, FI_t should also be 0 for the same reason.

For Case 2 ($\varphi_{util}=0.75$, $FI_d=0.415$ and $FI_t=0.723$), the simulation results are plotted in Figs. 6 and 7. It can be clearly observed that the worst-case scenario associated with each index reaches

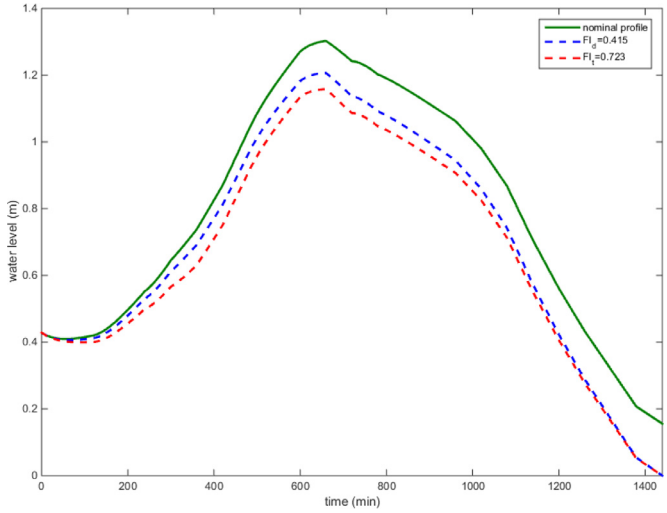

Fig. 6. The time profile of water level in the worst scenario ($\varphi_{util}=0.75$).

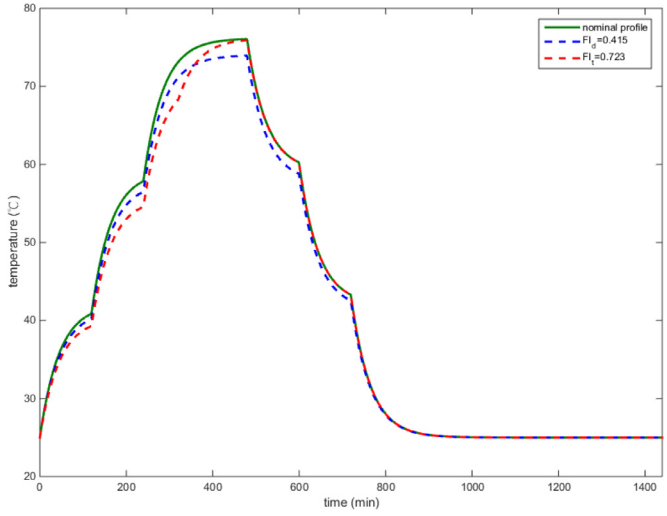

Fig. 7. The time profile of solar absorber outlet temperature in the worst scenario ($\varphi_{util}=0.75$).

the lower bound of water level in the distillate tank at the end of operation time. It is also found that the latter index ($FI_t=0.723$) is caused by the deviation of the solar irradiation rate from its nominal value to its lower bound between 2 and 321 min and the deviation of the water demand from its nominal value to its upper bound between 2 and 704 min at the same time. If a target flexibility value of 1 is desired, a feasible method is to increase the exposed area of solar absorber from 246.1 to 280.6 m^2 for improving the dynamic index and to 255.0 m^2 for temporal index. On the other hand, it is also feasible to achieve the flexibility target by adjusting the initial water level in distillate tank from 0.4285 to 0.648 m for improving the dynamic index and to 0.488 m for temporal index.

For Case 3 ($\varphi_{util}=1$, $FI_d=1.077$), the corresponding dynamic flexibility index represents that the process is operable during the time horizon despite the fact that all uncertainties deviate from nominal value and the process can afford exceptional deviations. For the reason that the dynamic flexibility index is greater than 1, meaning that all expected deviations from nominal value are affordable, the computation of temporal flexibility index is unnecessary.

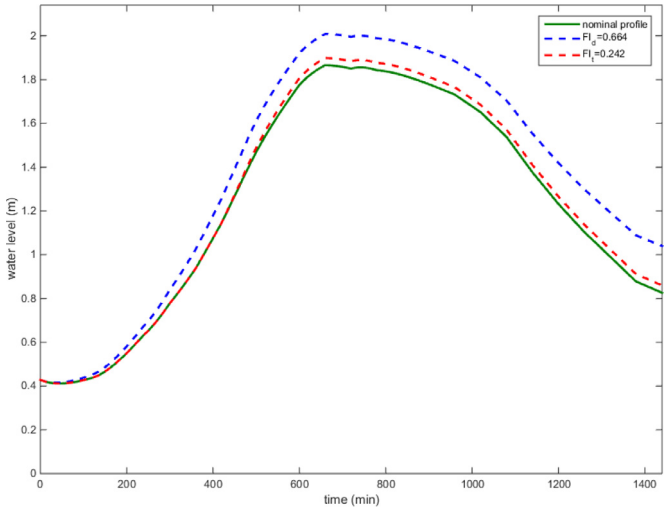

Fig. 8. The time profile of water level in the worst scenario ($\varphi_{util}=1.04$).

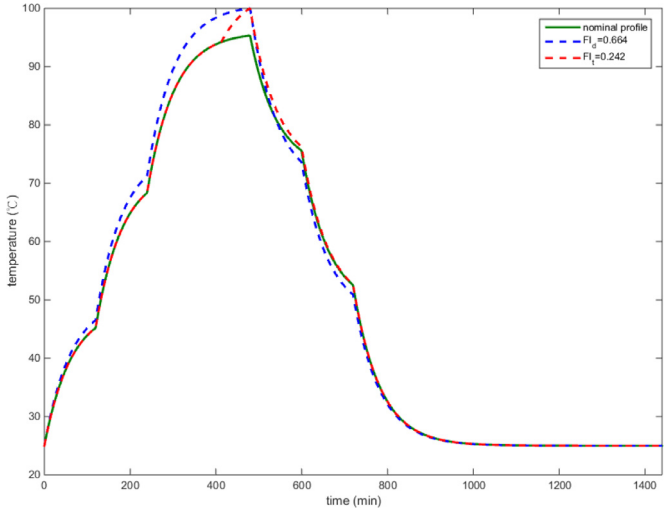

Fig. 9. The time profile of solar absorber outlet temperature in the worst scenario ($\varphi_{util}=1.04$).

For Case 4 ($\varphi_{util}=1.04$, $FI_d=0.664$ and $FI_t=0.242$), the simulation results can be seen in Figs. 8 and 9. It can be noted that the worst-case scenario associated with each index reaches the upper bound of the outlet temperature of solar absorber at 480 min. It is also found that the latter index ($FI_t=0.242$) is caused by a deviation of the solar irradiation rate from its nominal value to its upper bound between 414 and 480 min. For the reason that it is difficult to control the uncertainty parameters in this system, the most feasible option to achieve the flexibility targets is to modify ϕ_{util} via adjusting the exposed area of solar absorber. If a target flexibility value of 1 is desired, the required exposed area of solar absorber should be reduced from 341.3 to 330.5 m^2 for improving the dynamic index and to 330.6 m^2 for temporal index.

6.2.3. Computation performance

The computation performance of the proposed method has also been compared with that of the extended vertex method developed by Kuo and Chang. [14] It was again found that these two approaches resulted in almost the same flexibility indices in every scenario. Table 3 lists the computation times needed in Cases 2 and 4. The trends in these data are essentially no different from those observed in Example 1. In other words, solving the proposed model to evaluate the temporal flexibility index can be much more efficient than the existing vertex method although this same approach may call for a longer time for computing the dynamic flexibility index.

Table 3
Computation times needed to evaluate the dynamic and temporal flexibility indices by solving two alternative models in Cases 2 and 4 of Example 2.

	FI_d (s)		FI_t (s)	
Programming model	Case 2	Case 4	Case 2	Case 4
KKT	6.7	111	3401	831
Vertex	5.9	6.8	141,939	1336

7. Conclusions

By rigorously deriving the KKT conditions of a dynamic programming model, a systematic methodology has been developed in this work to compute the dynamic and temporal flexibility indices. It can be also noted that, depending upon the availability of historical data and intrinsic nature of uncertainty in the particular application, FI_d or FI_t (or both) can be used to represent the operational flexibility of an unsteady process, and more economical and flexible designs can then be conjectured accordingly.

In evaluating dynamic and temporal flexibility indices by the existing method, [14] one may attempt to reduce the computation load by ignoring some of the vertexes based on heuristic insights of the given system. The theoretically-sound KKT conditions can be adopted to validate the short-cut solutions in this situation. Furthermore, the computation effort for FI_t can also be significantly reduced with the proposed solution approach.

Acknowledgment

This work is supported by the Ministry of Science and Technology of the ROC government under grant MOST 104-222-E-006-237-MY3.

Appendix

Symbol	Definition	Value	Type
A_{SA}	Exposed area of solar absorber	–	d
A_{MD}	Membrane area of AGMD module	40 m^2	d
A_{DT}	Cross-sectional area of distillate tank	0.35 m^2	d
$T_{SAout,max}$	Maximum outlet temperature of solar absorber	100 °C	d
$T^{max}_{f,HX,CLout}$	Maximum cold stream temperature at outlet of heat exchanger	100 °C	d
$T_{f,HX,CLin}$	Cold stream temperature at inlet of heat exchanger	25 °C	d
M_{SA}	Total mass of operating fluid in solar absorber	–	d
m_{STL}	Mass flow rate in thermal loop	36,000 kg/hr	d
m^{max}_{MD}	Maximum mass flow rate in membrane distillation loop	4950 kg/hr	d
Cp^{L}	Heat capacity of operating fluid	4200 J/kg°C	d
ρ	Distillate density	1000 kg/m^3	d
n_{AGMD}	Total number of standard AGMD modules	4	d
$STEC$	Specific thermal energy consumption constant	14,000 kJ/kg	d
$h_{DT,lo}$	Lower bound of liquid height in distillate tank	0 m	d
$h_{DT,up}$	Upper bound of liquid height in distillate tank	2.14 m	d

(*continued on next page*)

Symbol	Definition	Value	Type
I^{max}	Maximum solar irradiation rate per unit area	1320 W/m^2	d
φ_{util}	Energy utilization ratio	–	d
$T_{f,SAin}$	Inlet temperature of solar absorber	–	x
$T_{f,SAout}$	Outlet temperature of solar absorber	–	x
$T_{f,HX,HLout}$	Hot stream temperature at outlet of heatexchanger	–	x
$T_{f,HX,HLin}$	Hot stream temperature at inlet of heat exchanger	–	x
$T_{f,HX,CLout}$	Cold stream temperature at outlet of heat exchanger	–	x
m_{SA}	Mass flow rate of operating fluid in solar absorber	–	x
$\dot{m}_{f,HX,HL}$	Mass flow rate of hot stream in heat exchanger	–	x
N_{mem}	Distillate flux through AGMD membrane	–	x
h_{DT}	Liquid height in distillate tank	–	x
$\dot{m}_{f,MD}$	Mass flow rate in membrane distillation loop	–	z
I	Solar irradiation rate per unit area	–	θ
w_D	Outlet flow rate of distillate tank	–	θ

References

[1] Malcom A, Polan J, Zhang L, Ogunnaike BA, Linninger AA. Integrating system design and control using dynamic flexibility analysis. AIChE J 2007;53:2048.
[2] Lima FV, Georgakis C. Design of output constraints for model-based non-square controllers using interval operability. J Process Contr 2008;18:610.
[3] Lima FV, Georgakis C, Smith JF, Schnelle PD, Vinson DR. Operability-based determination of feasible control constraints for several high-dimensional non-square industrial processes. AIChE J 2009;55:1249.
[4] Lima FV, Jia Z, Ierapetritou M, Georgakis C. Similarities and differences between the concepts of operability and flexibility: the steady-state case. AIChE J 2010;56:702.
[5] Swaney RE, Grossmann IE. An index for operational flexibility in chemical process design part I: formulation and theory. AIChE J 1985;31:621.
[6] Swaney RE, Grossmann IE. An index for operational flexibility in chemical process design part II: computational algorithms. AIChE J 1985;31:631.
[7] Dimitriadis VD, Pistikopoulos EN. Flexibility analysis of dynamic system. Ind Eng Chem Res 1995;34:4451.
[8] Brengel DD, Seider WD. Coordinated design and control optimization of non-linear process. Comput Chem Eng 1992;16:861.
[9] Dimitriadis VD, Shah N, Pantelides CC. Modeling and safety verification of discrete/continuous processing systems. AIChE J 1997;43:1041.
[10] Zhou H, Li XX, Qian Y, Chen Y, Kraslawski A. Optimizing the initial conditions to improve the dynamic flexibility of batch processes. Ind Eng Chem Res 2009;48:6321.
[11] Adi VSK, Chang CT. A mathematical programming formulation for temporal flexibility analysis. Comput Chem Eng 2013;57:151.
[12] Adi VSK, Chang CT. SMDDS design based on temporal flexibility analysis. Desalination 2013;320:96.
[13] Adi VSK, Chang CT. Development of flexible designs for PVFC hybrid power systems. Renew Energ 2015;74:176.
[14] Kuo YC, Chang CT. On heuristic computation and application of flexibility indices for unsteady process design. Ind Eng Chem Res 2016;55:670.